J. Fluid Mech. (1990), *vol.* 214, *pp.* 517–534
Printed in Great Britain

Chaotic advection of irrotational flows and of waves in fluids

By S. M. COX, P. G. DRAZIN, SUSAN C. RYRIE AND K. SLATER
School of Mathematics, University Walk, Bristol BS8 1TW, UK

(Received 4 May 1989)

This paper treats the kinematics of particles advected passively by flow of an incompressible fluid. It is shown that for steady irrotational flow without circulation, and for many monochromatic waves in a fluid the particle paths are not chaotic, i.e. do not depend sensitively on initial conditions. However, if the flow is a time-periodic potential flow or a superposition of waves then the particle paths may be chaotic. This is shown by the application of the theory of Melnikov to the breakup of a heteroclinic orbit (which connects two stagnation points and may bound a region of closed streamlines) and the onset of chaos in two examples of two-dimensional flow. The first example is a simple unbounded irrotational flow comprising a steady flow with two stagnation points which has a time-periodic perturbation. The second example is of two Rossby waves with a mean zonal flow; the particle paths are examined geometrically and numerically, and consequences for pollutant dispersion are discussed in physical terms. Also the combination of the effects of chaotic advection and molecular diffusion on the transport of a solute are examined.

1. Introduction

Arnol'd (1965) and Hénon (1966) were the first to recognize that particle paths in a smooth laminar flow may be chaotic. This profound qualitative difference between the Eulerian and Lagrangian properties of a flow has surprised many experienced research workers in fluid mechanics. However, it is not surprising to those familiar with the Lorenz (1963) system, namely

$$\frac{\mathrm{d}\boldsymbol{x}}{\mathrm{d}t} = \boldsymbol{u} \quad \text{and} \quad \boldsymbol{u}(\boldsymbol{x}) = (\sigma(y-x), rx-y-zx, \ -bz+xy), \tag{1.1}$$

if they regard the system as the equation of motion of the fluid particle at $\boldsymbol{x}(t)$ in the given flow with velocity $\boldsymbol{u}$ in three-dimensional physical space, rather than as an equation of evolution in a phase space; then the velocity field is steady, smooth and simple (albeit of little physical interest because of its form of compressibility) although the particle paths may be chaotic for certain values of the parameters σ, r and b. This phenomenon whereby a flow is laminar and some particle paths are chaotic is sometimes called *Lagrangian turbulence*, but we prefer the name *chaotic advection*, coined by Aref (1984), because the *flow* is not turbulent.

Arnol'd (1965), Hénon (1966) and Dombre *et al.* (1986) have demonstrated chaotic advection for Beltrami flows. We shall demonstrate it for two other important classes of flows – irrotational flows and waves in fluids. Although many irrotational flows are of little direct practical value, they are important in our understanding of flows of a slightly viscous fluid. Jones & Aref (1988) have already shown that one irrotational flow may give rise to chaotic advection. We shall use well-known tools of the theory of dynamical systems to show more generally why an irrotational flow may give rise to chaotic advection, and analyse an illustrative example in §2.

Waves in fluids arise in many branches of fluid mechanics. Most of the waves are important physically. Many are not only simple explicit solutions of the governing linearized equations of motion but also exact solutions of the nonlinear equations (cf. Craik & Criminale 1986). Are their particle paths chaotic? We shall address this question in §3, demonstrating some general as well as particular results, which describe the mechanism whereby waves disperse particles longitudinally. This mechanism may be viewed as a development of Taylor's (1953) pioneering theory of the longitudinal dispersion of a solute. Again, we shall find the dispersion of a passive tracer due to the pseudo-randomness of the stretching and folding associated with a laminar flow when the particle paths are chaotic, a mechanism different but analogous to that in the theory of turbulent flow (cf. Batchelor 1959). We shall examine some of the additional effects due to molecular diffusion in §4.

Throughout the paper we shall take each flow as given in Eulerian variables. Thus we shall assume the dynamics of the flow to be given and investigate some of the kinematics. The assumed flow may or may not have been found by linearizing the equations of motion: it is important to recognize the distinction between linearization of the equations of motion to find the Eulerian velocity field $\boldsymbol{u}$ and the linearity of the field $\boldsymbol{u}$ as a function of $\boldsymbol{x}$. Of course, the former does not imply the latter, so that a linearized wave field may produce chaotic advection. The geometrical arguments we use show that chaotic advection may occur whether, in deriving the velocity field, the equations of motion are linearized or not, because it is the topological character of the field that is important.

2. Irrotational flow

For an irrotational flow with velocity $\boldsymbol{u} = \boldsymbol{\nabla}\phi$ the particle paths are given by

$$\frac{\mathrm{d}\boldsymbol{x}}{\mathrm{d}t} = \boldsymbol{\nabla}\phi. \tag{2.1}$$

For a steady flow the potential ϕ is independent of the time t, and (2.1) implies that each fluid particle moves in the direction where ϕ increases most rapidly, i.e. moves 'up' the curve of steepest ascent of the equipotentials. Therefore, if there is no circulation, i.e. if the domain of flow is simply connected or if the domain is multiply connected but the flow is acyclic, the particle moves towards a maximum of ϕ. (By Earnshaw's theorem (Batchelor 1967, p. 384), for an incompressible fluid with $\boldsymbol{\nabla}\cdot\boldsymbol{u} = 0$ this maximum must lie at a boundary of the flow, at a singularity such as a sink, or at infinity.) Thus the paths of the particles are not chaotic.

It follows that chaotic advection for irrotational flows without circulation is possible only for two- or three-dimensional unsteady flows. In a sense it is possible to make particle paths chaotic by specifying ϕ and hence $\boldsymbol{u} = \boldsymbol{\nabla}\phi$ as a chaotic function of t for this purpose. Certainly we can make one particle follow any given integrable path in space by this mathematical method. Such chaos seems too artificial to be of interest, and we shall soon see that chaos can arise more naturally, so let us suppose that ϕ has period T and, for definiteness and simplicity, that there is two-dimensional flow of an incompressible fluid. Thus we assume that $\phi(x, y, t+T)$

$= \phi(x,y,t)$ for all t, and $\nabla^2\phi = 0$, and enquire whether chaotic particle paths are possible.

First examine the streamlines $\psi(x,y,t) = \text{constant}$ at each instant t, where the stream function ψ is such that $\phi_x = -\psi_y$ and $\phi_y = \psi_x$. (Recall that a streamline of an unsteady flow is in general not a particle path.) The critical points of the flow are the stagnation points where $\boldsymbol{\nabla}\phi = \mathbf{0}$. Without loss of generality, let such a point be instantaneously at the origin. Then, for a smooth flow, Maclaurin's theorem gives

$$\phi = \phi_0 + \tfrac{1}{2}(ax^2 + 2hxy - ay^2) + O(\boldsymbol{x}^3) \tag{2.2}$$

and
$$\psi = \psi_0 + \tfrac{1}{2}(hx^2 - 2axy - hy^2) + O(\boldsymbol{x}^3) \quad \text{as} \quad \boldsymbol{x} \to \mathbf{0} \tag{2.3}$$

for some functions ϕ_0, ψ_0, a and h of t. The critical point is therefore in general a saddle point with streamlines locally like rectangular hyperbolae. The topology of the streamlines for flow without circulation is now apparent. No streamline is closed. Each streamline goes to a boundary (or infinity), a saddle point or a singularity. There is an arbitrary number of saddle points and singularities linked by streamlines from one to another or to a boundary.

Jones & Aref (1988) have taken an irrotational two-dimensional flow with an oscillating source and sink and demonstrated chaos numerically, as well as other interesting fundamental phenomena. We shall examine another specific example in detail in order to investigate the possibility of chaos mathematically, identify the mechanism clearly and then discuss longitudinal dispersion by waves.

So consider the family of flows with potential

$$\phi(x,y,t) = \phi_0(x,y) + \epsilon\phi_1(x,y,t), \tag{2.4}$$

where
$$\phi_0(x,y) = -\cos x \cosh y \quad \text{and} \quad \phi_1(x,y,t) = y \sin \omega t \tag{2.5}$$

for a given frequency $\omega = 2\pi/T$ and parameter ϵ. Then

$$\frac{\mathrm{d}x}{\mathrm{d}t} = \sin x \cosh y \quad \text{and} \quad \frac{\mathrm{d}y}{\mathrm{d}t} = -\cos x \sinh y + \epsilon \sin \omega t. \tag{2.6}$$

The portraits of the streamlines for $t = 0$ (and all ϵ, and also for all t when $\epsilon = 0$) and for $t = \pi/2\omega$, $\epsilon = 0.4$ are shown in figure 1; the streamlines for other values of t may be inferred by interpolation, and by extrapolation on using the system's period $2\pi/\omega$ and symmetry under the transformation $t \mapsto \pi/\omega - t$.

We may restrict attention to the region $0 \leqslant x \leqslant \pi$ because the flows have period 2π in x, and are symmetric about $x = 0$, which is both a particle path and a streamline for all t and ϵ. To investigate the possibility of chaotic particle paths for $\epsilon \neq 0$, we treat this case by perturbing the flow for $\epsilon = 0$, using Melnikov's method (see e.g. Guckenheimer & Holmes 1983, §4.5).

The unperturbed system,

$$\frac{\mathrm{d}x}{\mathrm{d}t} = \sin x \cosh y, \quad \frac{\mathrm{d}y}{\mathrm{d}t} = -\cos x \sinh y, \tag{2.7}$$

has a sequence of stagnation points at $(n\pi, 0)$ for $n = 0, \pm 1, \pm 2, \ldots$ with heteroclinic orbits between adjacent points. These stagnation points are saddle points of the streamlines. The orbit between $(0,0)$ and $(\pi,0)$ is given by

$$\boldsymbol{q}_0(t) = (x_0(t), y_0(t)), \tag{2.8}$$

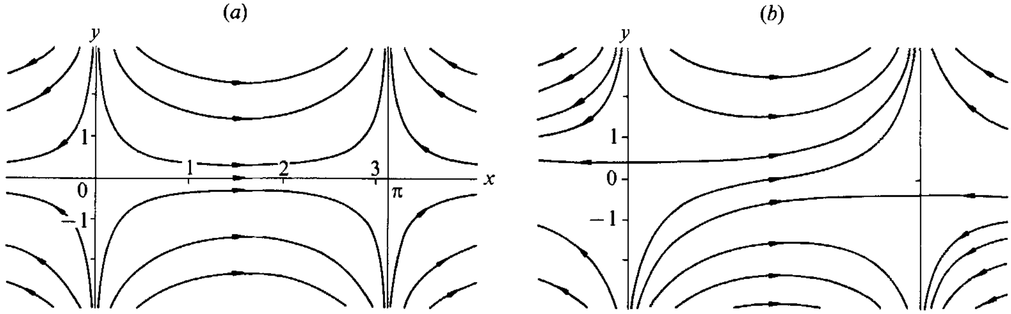

FIGURE 1. (*a*) The particle paths (2.7), which coincide with the streamlines of the unperturbed mean flow and with those of the perturbed flow (2.6) at $t = 0$; (*b*) the streamlines of the perturbed flow at $t = \pi/2\omega$ for $\epsilon = 0.4$. Note that the lines $x = 0$, π are streamlines for all t, ϵ.

where integration of (2.7) gives

$$\sin x_0(t) = \operatorname{sech}[t + \ln\{\tan \tfrac{1}{2}x_0(0)\}] \quad \text{and} \quad y_0(t) = 0 \quad \text{for all } t. \tag{2.9}$$

This heteroclinic orbit exists because the unstable manifold $W_0^{\mathrm{u}}(0,0)$ of $(0,0)$ and the stable manifold $W_0^{\mathrm{s}}(\pi,0)$ of $(\pi,0)$ for the unperturbed system (2.7) coincide and equal the line segment $y = 0$, $0 \leqslant x \leqslant \pi$ (see figure 1*a*). Here the unstable manifold $W_0^{\mathrm{u}}(0,0)$ essentially means the streamline that leaves $(0,0)$ and the stable manifold $W_0^{\mathrm{s}}(\pi,0)$ means the streamline that goes into $(\pi,0)$.

For the perturbed system it is sometimes convenient to consider not (2.6) but an equivalent autonomous system of third order, namely the suspended system

$$\left.\begin{aligned} \frac{\mathrm{d}x}{\mathrm{d}t} &= \sin x \cosh y, \\ \frac{\mathrm{d}y}{\mathrm{d}t} &= -\cos x \sinh y + \epsilon \sin \omega\theta, \\ \frac{\mathrm{d}\theta}{\mathrm{d}t} &= 1, \end{aligned}\right\} \tag{2.10}$$

where $(x, y, \theta) \in [0, \pi] \times \mathbb{R} \times S^1$. (Here $S^1 = \mathbb{R}/T$ is the circle of length T, and $T = 2\pi/\omega$ is the period of the oscillating flow.) We identify θ with t by appropriate choice of the origin. A useful instrument to probe this system is the Poincaré map $\mathrm{P}_\epsilon^{t_0}\colon \Sigma^{t_0} \to \Sigma^{t_0}$ defined by

$$\Sigma^{t_0} = \{(x, y, \theta) \in [0, \pi] \times \mathbb{R} \times S^1 : \theta = t_0 \in [0, T)\} \tag{2.11}$$

and

$$\mathrm{P}_\epsilon^{t_0}\colon\ (x(t_0), y(t_0), t_0) \mapsto (x(t_0 + T), y(t_0 + T), t_0). \tag{2.12}$$

This is effectively a stroboscopic map of the plane of flow which gives the new position of each fluid particle after a time T has elapsed. For simplicity we choose to set $t_0 = 0$: we may do this without loss of generality by changing the phase in (2.6).

Now P_ϵ^0 has invariant lines $x = 0$ and $x = \pi$. On $x = 0$, P_ϵ^0 can be shown to be a contraction mapping. Moreover, since $\mathrm{d}|y|/\mathrm{d}t \leqslant 0$ on $x = 0$ wherever $|y| \geqslant \operatorname{arcsinh}|\epsilon|$, P_ϵ^0 maps the line segment $I^0 = \{(x, y) : x = 0,\ |y| \leqslant \operatorname{arcsinh}|\epsilon|\}$ into itself. Therefore, by Banach's contraction mapping theorem (cf. Griffel 1981, §5.2), P_ϵ^0 has a unique fixed point $\boldsymbol{p}_0$ in I^0 whose position will vary with ϵ. Similarly, consideration of the inverse map $(\mathrm{P}_\epsilon^0)^{-1}$ on $x = \pi$ shows that P_ϵ^0 has a unique fixed point $\boldsymbol{p}_\pi$ in the line segment $I^\pi = \{(x, y):\ x = \pi,\ |y| \leqslant \operatorname{arcsinh}|\epsilon|\}$. When $\epsilon = 0$, $\boldsymbol{p}_0$ and $\boldsymbol{p}_\pi$ become the stagnation points, $(0,0)$ and $(\pi,0)$ respectively, of the unperturbed two-dimensional flow; the unstable manifold of $\boldsymbol{p}_0$ is then identified with $W_0^{\mathrm{u}}(0,0)$ and the stable manifold of $\boldsymbol{p}_\pi$ with $W_0^{\mathrm{s}}(\pi,0)$. As we have seen, these coincide along $y=0$. However, it turns out that when $\epsilon \neq 0$ the manifolds $W_\epsilon^{\mathrm{u}}(\boldsymbol{p}_0)$ and $W_\epsilon^{\mathrm{s}}(\boldsymbol{p}_\pi)$ of the fixed points of the Poincaré map no longer coincide. Here $W_\epsilon^{\mathrm{u}}(\boldsymbol{p}_0)$ is defined essentially as the curve along which points leave $\boldsymbol{p}_0$ by iteration of the map P_ϵ^0, and $W_\epsilon^{\mathrm{s}}(\boldsymbol{p}_\pi)$ as the curve along which points approach $W_\epsilon^{\mathrm{s}}(\boldsymbol{p}_\pi)$ similarly (cf. Guckenheimer & Holmes 1986). Remember that in the unsteady flow these manifolds are distinct from streamlines at each instant. We shall next apply Melnikov's method to determine the separation of the manifolds and, in particular, to find whether they intersect transversely when ϵ is small.

Let $x_m \in (0,\pi)$. Also note that the normal to $W_0^{\mathrm{u}}(0,0) = W_0^{\mathrm{s}}(\pi,0)$ at $(x_m,0)$ is the line $x=x_m$. Then the distance $d_\epsilon(x_m)$ between the intersections of $W_\epsilon^{\mathrm{u}}(\boldsymbol{p}_0)$ and $W_\epsilon^{\mathrm{s}}(\boldsymbol{p}_\pi)$ with the normal at $(x_m,0)$ is given by

$$d_\epsilon(x_m) = \frac{\epsilon M(x_m)}{|\boldsymbol{u}_0(x_m,0)|} + O(\epsilon^2) \quad \text{as} \quad \epsilon \to 0, \tag{2.13}$$

where the Melnikov function M is defined by

$$M(x_m) = \int_{-\infty}^{\infty} \{\boldsymbol{u}_0(\boldsymbol{q}_0(t)) \wedge \boldsymbol{u}_1(\boldsymbol{q}_0(t),t)\}\cdot\boldsymbol{k}\,\mathrm{d}t, \tag{2.14}$$

$\boldsymbol{u}_0 = \boldsymbol{\nabla}\phi_0$, $\boldsymbol{u}_1 = \boldsymbol{\nabla}\phi_1$, $\boldsymbol{k}$ is the unit vector parallel to the z-axis, and $\boldsymbol{q}_0(t)$ is that heteroclinic orbit of the unperturbed flow which passes through $x=x_m$ at $t=0$. Thus M depends on x_m through the initial condition for $\boldsymbol{q}_0$, i.e. through

$$\boldsymbol{q}_0(0) = (x_m,0). \tag{2.15}$$

For the system (2.6) we accordingly deduce that

$$\begin{aligned} M(x_m) &= \int_{-\infty}^{\infty} \sin x_0(t)\sin \omega t\,\mathrm{d}t \\ &= -\int_{-\infty}^{\infty} \operatorname{sech} t\cos\omega t\,\mathrm{d}t\,\sin\{\omega\ln(\tan\tfrac{1}{2}x_m)\} \\ &= -\pi\sin\{\omega\ln(\tan\tfrac{1}{2}x_m)\}\operatorname{sech}\tfrac{1}{2}\pi\omega. \end{aligned} \tag{2.16}$$

This Melnikov function has simple zeros and so we conclude that the manifolds $W_\epsilon^{\mathrm{u}}(\boldsymbol{p}_0)$ and $W_\epsilon^{\mathrm{s}}(\boldsymbol{p}_\pi)$ intersect transversely (and do so a countable infinity of times near $x_m = 0$ or π). It also gives the distance function as

$$d_\epsilon(x_m) = -\frac{\epsilon\pi\sin\{\omega\ln(\tan\frac{1}{2}x_m)\}}{\sin x_m\cosh\frac{1}{2}\pi\omega} + O(\epsilon^2) \quad \text{as} \quad \epsilon\to 0. \tag{2.17}$$

This agrees well with the separation between the manifolds found by integrating the system (2.6), even for values of ϵ which are not small (we have used values $\epsilon \lesssim 10$ for various values of ω). Figure 2 shows $W_\epsilon^{\mathrm{u}}(\boldsymbol{p}_0)$ and $W_\epsilon^{\mathrm{s}}(\boldsymbol{p}_\pi)$ for $\epsilon=3$ and $\omega=4$ to illustrate this; the Melnikov asymptotic calculations of $W_\epsilon^{\mathrm{u}}(\boldsymbol{p}_0)$ and $W_\epsilon^{\mathrm{s}}(\boldsymbol{p}_\pi)$ to order ϵ agree so well with the direct integrations of the system that they would be indistinguishable in figure 2.

This is not just a formal piece of mathematics, for it is valuable in helping us to understand how particles are advected by the unsteady flow. All the fluid above the curve $W_\epsilon^{\mathrm{u}}(\boldsymbol{p}_0)$ comes from near $x=0$ and $y=\infty$, and all the fluid below comes from near $x=0$ and $y=-\infty$; also all the fluid above the curve $W_\epsilon^{\mathrm{s}}(\boldsymbol{p}_\pi)$ goes to near $x=\pi$

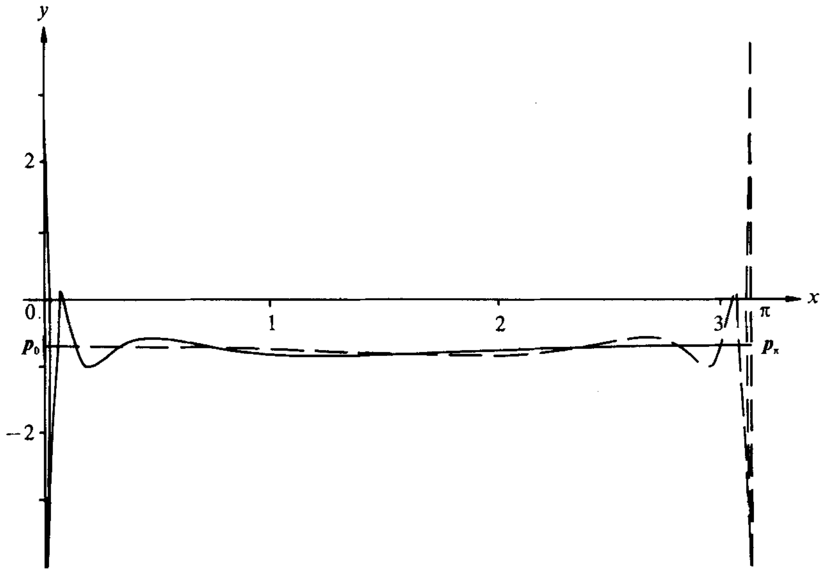

FIGURE 2. The stable manifold $W^s_\epsilon(p_\pi)$ (denoted by a continuous curve) and the unstable manifold $W^u_\epsilon(p_0)$ (denoted by a broken curve) of the Poincaré map when $\epsilon = 3$ and $\omega = 4$, i.e. when $\phi(x, y, t) = -\cos x \cosh y + 3y \sin 4t$.

and $y = \infty$, and all the fluid below goes to near $x = \pi$ and $y = -\infty$. Thus fluid above both $W^u_\epsilon(p_0)$ and $W^s_\epsilon(p_\pi)$ comes from and goes to $y = \infty$; fluid below $W^u_\epsilon(p_0)$ and $W^s_\epsilon(p_\pi)$ comes from and goes to $y = -\infty$; whereas fluid in the 'lobes' between $W^u_\epsilon(p_0)$ and $W^s_\epsilon(p_\pi)$ comes from $y = \pm\infty$ and goes to $y = \mp\infty$ respectively, so it is the exchange of fluid in alternate lobes which makes up the transport across the separatrix of the basic flow, due to the oscillation (see figure 2). The area of a lobe can be calculated to order ϵ by integrating the distance $d_\epsilon(x_m)$ between two of its adjacent zeros (cf. Rom-Kedar 1989; Ryrie 1990). In this flow we find, for each lobe, the area

$$A_\epsilon = \frac{2\pi\epsilon}{\omega \cosh(\frac{1}{2}\pi\omega)} + O(\epsilon^2) \quad \text{as} \quad \epsilon \to 0.$$

The areas of all the lobes are *exactly* the same, owing to the incompressibility of the fluid and to the absence of a net flux from $y = -\infty$ to $y = +\infty$. Then, when the boundary between the upper and lower regions is appropriately defined (cf. Ryrie 1990), exactly one lobe of fluid is exchanged per period T of the flow, so that the area of fluid moving from the upper (or lower) region to the lower (or upper, respectively) region per period T is just A_ϵ. Thus the Melnikov theory provides information about the transport properties of the flow.

To illustrate this exchange of fluid, figure 3 shows the second and fourth iterates of a line segment $L = \{(x, y): x = 0.002, -5.1 < y < 4.0\}$ under the Poincaré map P^0_ϵ, again for $\epsilon = 3$ and $\omega = 4$. The figure does not show L itself because L would be indistinguishable from the y-axis. These iterates, then, mark the position of the line of fluid particles after two and four periods of the flow, i.e. after times π and 2π. The second iterate $(\mathrm{P}^0_\epsilon)^2 L$ shows that L has been 'sucked' towards $W^u_\epsilon(p_0)$, for the flow is approximately that for the case $\epsilon = 0$ shown in figure 1. However, the fourth iterate shows (and subsequent iterates would show more dramatically) how the line segment becomes contorted near $x = \pi$, where $W^s_\epsilon(p_\pi)$ straightens and $W^u_\epsilon(p_0)$ bends. Close to $x = 0$, the curve $W^s_\epsilon(p_\pi)$ bows and intersects vertical lines a number of times (and, in

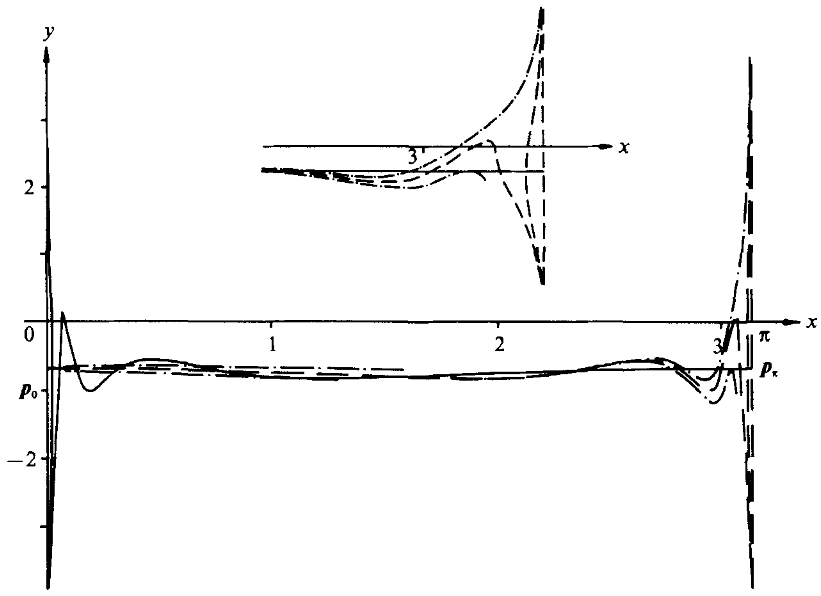

FIGURE 3. Iterates of the Poincaré map on the line segment $L = \{(x,y): x = 0.002, -5.1 < y < 4\}$ when $\epsilon = 3$ and $\omega = 4$. The stable manifold $W^s_\epsilon(p_\pi)$ of figure 2 is denoted by a continuous curve, the unstable manifold $W^u_\epsilon(p_0)$ by a broken curve, and the second and fourth iterates of L by chained curves. An enlargement of a detail, which shows the fourth iterate of L, i.e. the fluid particles of L after an interval 2π, is shown in the inset.

fact, here intersects L six times). The invariance of $W^s_\epsilon(p_\pi)$ ensures that each subsequent iterate intersects $W^s_\epsilon(p_\pi)$ the same number of times, as seen in figure 3: these intersections divide L into segments which are swept far upwards (or downwards) as $t \to \infty$ according to whether they lie above (or below) $W^s_\epsilon(p_\pi)$. The *flow* is not chaotic but there is sensitive dependence of particle paths on initial conditions near the line $x = 0$. For, given any non-vertical straight line L_0 through p_0 there exist sequences $\{x_n\}$ where (i) $x_n \in L_0$ for $n = 1, 2, \ldots$ and (ii) $x_n \to p_0$ monotonically as $n \to \infty$, such that

$$\lim_{m\to\infty} (\mathrm{P}^0_\epsilon)^m x_n = \begin{cases} (\pi, +\infty) & \text{if } n \text{ is odd} \\ (\pi, -\infty) & \text{if } n \text{ is even.} \end{cases}$$

In short, neighbouring particles near $x = 0$ may be separated and swept in different directions to $y = \pm\infty$ near $x = \pi$, according to which lobes between the manifolds they lie in. Indeed, such a result is valid for most curves intersecting the line $x = 0$. This advection is chaotic in the sense of sensitive dependence on initial conditions, because points near p_0 are scattered. (Recall that sensitive dependence on initial conditions is associated not just with exponential separation of neighbouring particles but also with the complicated nature of the boundary separating orbits of different qualitative behaviour.)

This serves as a simple example of an effect whereby an oscillation of a flow advects some particles across a separatrix of the steady mean flow. The effect is an important element in the mixing of fluids, to which the irrotationality of the flow is not directly material. A realistic, but more complicated, example of this can be seen in the diffusion of fluid particles in the axial direction when there are wavy Taylor vortices between two rotating cylinders (Broomhead & Ryrie 1988). In this example the spatial periodicity of the flow and the existence of closed streamlines are essential features of the mechanism of diffusion (cf. Ryrie 1990). However, irrotational flows without circulation do not have closed streamlines and so seem unlikely to lead to diffusion by means of chaotic advection.

3. Waves in fluids

We shall here make a few general remarks about chaotic advection due to waves in fluids, and then consider the case of the superposition of two Rossby waves in detail. It is well known that chaotic advection does not occur for two-dimensional steady flows, because the Poincaré–Bendixson theorem excludes the possibility of chaotic solutions of a two-dimensional autonomous differential system. This excludes chaotic advection by a wave which may be reduced to rest in some two-dimensional frame by a Galilean transformation, and so by all the steadily propagating two-dimensional waves which figure so prominently in the literature of fluid mechanics. So we must consider two-dimensional waves which cannot be reduced to rest, and three-dimensional waves in order to find chaotic particle paths.

For a single wave propagating in a fluid we may choose a coordinate frame moving with the wave. Then the equation of particle paths takes the autonomous form

$$\frac{\mathrm{d}\boldsymbol{x}}{\mathrm{d}t} = \boldsymbol{u}(\boldsymbol{x}). \tag{3.1}$$

We usually find the velocity field $\boldsymbol{u}$ by linearizing the governing equations of the flow, using the method of normal modes, and separating one or more of the space variables. This often yields $\boldsymbol{u} = (u, v, w)$ with two velocity components of the form

$$v(\boldsymbol{x}) = f(x)\, g_2(y,z) \quad \text{and} \quad w(\boldsymbol{x}) = f(x)\, g_3(y,z). \tag{3.2}$$

Important examples of such three-dimensional waves in a fluid are the baroclinic waves which model the large-scale instability of the winds in the middle latitudes (Eady 1949), and linear Rayleigh–Bénard convection (cf. Lorenz 1963). For such flows

$$\begin{aligned} \frac{\mathrm{d}z}{\mathrm{d}y} &= \frac{\mathrm{d}z}{\mathrm{d}t}\bigg/\frac{\mathrm{d}y}{\mathrm{d}t} = \frac{w}{v} \\ &= \frac{g_3(y,z)}{g_2(y,z)} \end{aligned} \tag{3.3}$$

on a particle path, and so z may be expressed as a function of y and hence eliminated from the equation (3.1) of particle paths. This reduces the system to a two-dimensional one and so excludes the possibility of chaotic advection. A somewhat similar 'non-chaos theorem' follows when x, y, z represent any trio of curvilinear coordinates in any order.

These results leave few examples in the literature of waves in fluids which may have chaotic advection. However, the results do not apply when two or more linear waves are superposed or there is a single three-dimensional nonlinear wave with higher harmonics such that the velocity field $\boldsymbol{u}(\boldsymbol{x}, t)$ does not give integrable equations like (3.3). These flows are, of course, more realistic than a single monochromatic sinusoidal wave in a fluid. With this in mind, we choose an illustrative example of Rossby waves which model large-scale barotropic winds and ocean currents in middle latitudes.

With a basic zonal (i.e. eastward) velocity $U\boldsymbol{i}$ on the β-plane of Rossby, it is well known (cf. Holton 1979, §7.5) that the basic flow and a Rossby wave have stream function $\psi(x,y,t) = -Uy + \mathrm{Re}\{A\,\mathrm{e}^{\mathrm{i}(kx+ly-\omega t)}\}$ for arbitrary complex amplitude A, real wavenumbers k and l, and dispersion relation $\omega = Uk - \beta k/(k^2+l^2)$. It is noteworthy that a single Rossby wave gives an exact solution of the nonlinear equations although linearization is needed in general to superpose Rossby waves.

We shall suppose that the flow is bounded by rigid vertical walls along two latitude circles. This artifice is widely used in meteorology and may be justified as a model of waves that are evanescent at high and low latitudes owing to shear of the zonal mean flow (cf. Drazin, Beaumont & Coaker 1982). Using dimensionless variables, we take the equations of these circles as $y = 0, 1$. For our example, we superpose two Rossby waves having $l = \pi$ (for the lowest meridional mode), the first having real amplitude A and zonal wavenumber $k = 2\pi$ (for the lowest mode) and the second having amplitude ϵA and $k = 4\pi$ (for the second zonal mode). We shall also make a Galilean transformation that reduces the first wave to rest. This gives $\omega = 0$ for the first wave and thence $U = \beta/5\pi^2$: the dispersion relation for the second wave then gives $\omega = 48\beta/85\pi$. In all our numerical calculations we shall set $\omega = 2\pi$ for the second wave, so that the period of the flow is $T = 1$, and hence take $\beta = 85\pi^2/24$ and $U = 17/24$. Thus we consider the class of flows with

$$\psi(x,y,t) = \psi_0(x,y) + \epsilon\psi_1(x,y,t), \tag{3.4}$$

where $\psi_0(x,y) = -Uy + A\cos 2\pi x \sin \pi y$, $\psi_1(x,y,t) = A\cos(4\pi x - \omega t)\sin \pi y$ and ϵ is a real parameter which we shall take to be small. Then ψ_0 represents a steady uniform flow and a wave, and ψ_1 a time-dependent wave perturbation.

As in §2 the equations of a particle path are of the form

$$\frac{\mathrm{d}\boldsymbol{x}}{\mathrm{d}t} = \boldsymbol{u}_0(\boldsymbol{x}) + \epsilon \boldsymbol{u}_1(\boldsymbol{x}, t), \tag{3.5}$$

and in detail they are

$$\frac{\mathrm{d}x}{\mathrm{d}t} = U - \pi A \cos 2\pi x \cos \pi y - \pi\epsilon A \cos(4\pi x - \omega t)\cos \pi y, \tag{3.6}$$

$$\frac{\mathrm{d}y}{\mathrm{d}t} = -2\pi A \sin 2\pi x \sin \pi y - 4\pi\epsilon A \sin(4\pi x - \omega t)\sin \pi y. \tag{3.7}$$

Note that the two rigid boundaries, i.e. the walls $y = 0, 1$, are invariant lines of the flow for all ϵ. Also the Eulerian velocity field has period 1 in x. Therefore we need only consider the domain of flow $0 \leqslant x, y \leqslant 1$. We may identify $x = 1$ with $x = 0$ so that a particle leaving this domain at $x = 1$ reappears at $x = 0$, or vice versa; this corresponds to flow on a cylindrical surface, such as the surface of the Earth in mid-latitudes. Note that the system (3.6), (3.7) is invariant under the transformations $\mathrm{T}_1\colon x \mapsto x + \frac{1}{2}$, $y \mapsto 1 - y$, $t \mapsto t + \frac{1}{2}T$, and $\mathrm{T}_2\colon x \mapsto 1 - x, y \mapsto y$, $t \mapsto -t$.

Consider first the unperturbed flow, $\boldsymbol{u}_0$. When $A < U/\pi$ the zonal velocity dominates the first Rossby wave so that the component of the basic velocity in the direction of the channel, i.e. the x-component u_0, is positive everywhere. However, when $A > U/\pi$ there are stagnation points and regions of recirculation. These regions are separated from the main stream by dividing streamlines, which, in the context of the theory of dynamical systems, are heteroclinic orbits. This is illustrated in figure 4 for $A = 1/\pi$ ($> U/\pi = 17/24\pi$). There are six stagnation points in the flow, denoted by $\boldsymbol{p}_1$, $\boldsymbol{p}_2$, $\boldsymbol{p}_3$, $\boldsymbol{p}_4$, $\boldsymbol{c}_1$ and $\boldsymbol{c}_2$: of these $\boldsymbol{c}_1$ and $\boldsymbol{c}_2$ are centres and the rest are hyperbolic saddle points. The saddle points $\boldsymbol{p}_1$ and $\boldsymbol{p}_2$ are joined by a streamline, Γ_0,

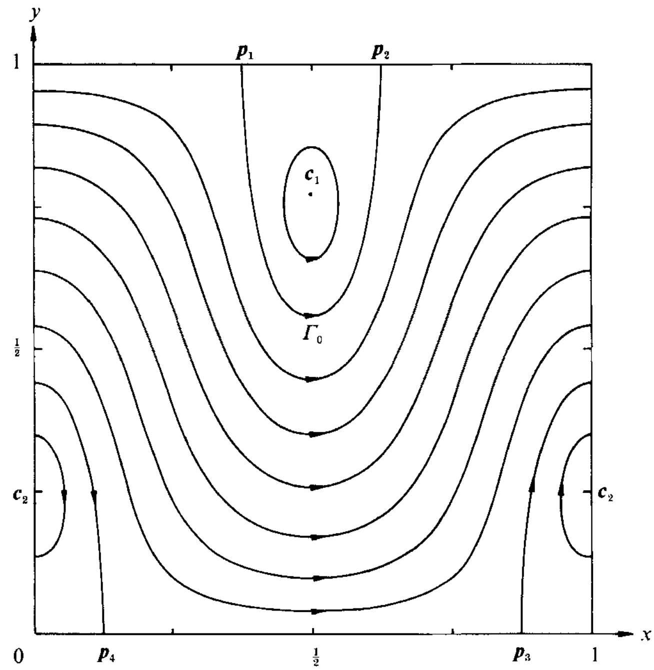

FIGURE 4. Streamlines of the steady unperturbed flow (3.8) with $U = 17/24$, $A = 1/\pi$, showing the heteroclinic orbit Γ_0.

say: a streamline similarly joins $\boldsymbol{p}_3$ and $\boldsymbol{p}_4$. We shall consider here the structure of Γ_0 and its fate under the action of the perturbation. Symmetry of the flow under the transformation T_1 implies that the streamline connecting $\boldsymbol{p}_3$ and $\boldsymbol{p}_4$ will be affected in the same way.

As in §2, we note that the heteroclinic connection of the unperturbed system exists because the unstable manifold of $\boldsymbol{p}_1$ and the stable manifold of $\boldsymbol{p}_2$ coincide, i.e. $W_0^{\mathrm{u}}(\boldsymbol{p}_1) = W_0^{\mathrm{s}}(\boldsymbol{p}_{\mathrm{s}}) = \Gamma_0$. Since $\psi_0(\boldsymbol{p}_1) = -U = \psi_0(\boldsymbol{p}_2)$, the equation of Γ_0 is given by

$$\cos 2\pi x = -U(1-y)/A \sin \pi y. \tag{3.8}$$

It follows that the heteroclinic orbit is $\boldsymbol{q}_0(t) = (x_0(t), y_0(t))$, where

$$\frac{\mathrm{d}y_0}{\mathrm{d}t} = -2\pi\{A^2 \sin^2 \pi y_0 - U^2(1-y_0)^2\}^{\frac{1}{2}}, \tag{3.9}$$

$y_0 \neq 1$, and x_0 is determined from (3.8) after (3.9) is solved. As before, this heteroclinic orbit is broken by the perturbation. We shall explore this with the aid of the Poincaré map $\mathrm{P}_\epsilon^{t_0}: \Sigma^{t_0} \rightarrow \Sigma^{t_0}$, where here

$$\Sigma^{t_0} = \{(x, y, \theta) \in S^1 \times [0, 1] \times S^1 : \theta = t_0 \in [0, T)\}, \tag{3.10}$$

θ is the new variable in the suspended system, and the temporal period of the flow is $T = 2\pi/\omega$.

The stagnation points of the flow are fixed points of the map $\mathrm{P}_0^{t_0}$. For sufficiently small ϵ, there are corresponding fixed points of the map $\mathrm{P}_\epsilon^{t_0}$; indeed we find numerically that, for $\omega = 2\pi$, $\beta = 85\pi^2/24$ and $U = 17/24$, $\mathrm{P}_\epsilon^{t_0}$ has two saddle points on each wall for $0 < \epsilon < 0.5646$. We denote the two saddle points on the wall $y = 1$, by $\boldsymbol{p}_j(\epsilon) = (x_j(\epsilon), 1)$ for $j = 1, 2$. Note that because (3.6) and (3.7) are invariant under the transformation T_2, the map P_ϵ^0 has the symmetry $P_\epsilon^0(1-x, y) = (P_\epsilon^0)^{-1}(x, y)$. This implies that, on Σ^0, $x_2(\epsilon) = 1-x_1(\epsilon)$. Let the unstable and stable manifolds be $W_\epsilon^u(\boldsymbol{p}_1)$ and $W_\epsilon^s(\boldsymbol{p}_2)$ respectively. It follows that $W_\epsilon^u(\boldsymbol{p}_1)$ is the mirror image of $W_\epsilon^s(\boldsymbol{p}_2)$ in the line $x = \frac{1}{2}$. Therefore if $W_\epsilon^u(\boldsymbol{p}_1)$ intersects the line $x = \frac{1}{2}$ at some point, then $W_\epsilon^s(\boldsymbol{p}_2)$ intersects it at the same point. Then $W_\epsilon^u(\boldsymbol{p}_1)$ and $W_\epsilon^s(\boldsymbol{p}_2)$ intersect at least a countable infinity of times.

To determine whether the manifolds $W_\epsilon^u(\boldsymbol{p}_1)$ and $W_\epsilon^s(\boldsymbol{p}_2)$ intersect transversely for small ϵ, we adapt Melnikov's method of §2 to the present problem. Bertozzi (1988) has also applied Melnikov's method to similar flows, including Rossby waves, but with zero mean flux; this corresponds asymptotically to the limit as $A \to \infty$, although we see that it is not possible to reduce the basic Rossby wave to rest and have no mean zonal flow U, and that the mean flow, however weak, changes the topology of the unperturbed flow, thereby separating the two regions of closed streamlines.

Now, the Melnikov function can be expressed as

$$M(x_0(0), y_0(0), t_0) = I_c(x_0(0), y_0(0)) \cos(\omega t_0) + I_s(x_0(0), y_0(0)) \sin(\omega t_0), \tag{3.11}$$

where

$$I_c = -\pi^2 A^2 \int_{-\infty}^{\infty} [4U(\pi A)^{-1} \sin(4\pi x_0(t) - \omega t) \sin \pi y_0(t) - \{\tfrac{3}{2}\sin(2\pi x_0(t) - \omega t) + \tfrac{1}{2}\sin(6\pi x_0(t) - \omega t)\} \sin 2\pi y_0(t)]\, \mathrm{d}t \tag{3.12}$$

and

$$I_s = \pi^2 A^2 \int_{-\infty}^{\infty} [4U(\pi A)^{-1} \cos(4\pi x_0(t) - \omega t) \sin \pi y_0(t) - \{\tfrac{3}{2}\cos(2\pi x_0(t) - \omega t) + \tfrac{1}{2}\cos(6\pi x_0(t) - \omega t)\} \sin 2\pi y_0(t)]\, \mathrm{d}t. \tag{3.13}$$

This gives the distance d_ϵ between the intersections of the manifolds $W_\epsilon^u(\boldsymbol{p}_1)$ and $W_\epsilon^s(\boldsymbol{p}_2)$ with the normal to Γ_0 at $(x_0(0), y_0(0))$ as

$$d_\epsilon = \frac{\epsilon(I_c \cos \omega t_0 + I_s \sin \omega t_0)}{[U^2\{1+\pi(1-y_0(0)) \cot \pi y_0(0)\}^2 + 4\pi^2 A^2 \sin^2 \pi y_0(0) - 4\pi^2 U^2 (1-y_0(0))^2]^{\frac{1}{2}}} + O(\epsilon^2) \quad \text{as} \quad \epsilon \to 0. \tag{3.14}$$

Provided I_c and I_s are not both identically zero, the manifolds cease to coincide when $\epsilon \neq 0$ and intersect transversely on Σ^{t_0} near the values of $(x_0(0), y_0(0))$ at which the Melnikov function vanishes. Numerical calculations suggest that this proviso is satisfied generally. On setting $x_0(0) = \frac{1}{2}$, we deduce that $I_c = 0$ because the integrand is then an odd function of t; however, our numerical calculations suggest that in general $I_s \neq 0$. Thus the manifolds intersect near $x = \frac{1}{2}$ on Σ^0 as anticipated. Parts of the manifolds computed for $A = 1/\pi$, and $\epsilon = 0.01$, are shown in figure 5.

The similarity between the systems of §2 and this section is now apparent. The transverse intersection of the manifolds again leads us to deduce that the particle paths of the flow with the two Rossby waves are sensitive to initial conditions, with neighbouring particles near Γ_0 being quickly separated. However, here no particle may escape to infinity, so the chaos of some of the solutions of (3.5) can be seen with the aid of a Poincaré map. For all $\epsilon \neq 0$ there exist two chaotic regions associated with the broken heteroclinic orbits. For ϵ not too large there are also regular solutions, which lie on stable toroidal surfaces in the phase space of (x, y, θ). These tori act as barriers to the trajectories of the chaotic solutions. In particular, stable tori in the main stream form a 'zonal' barrier which separates the two chaotic

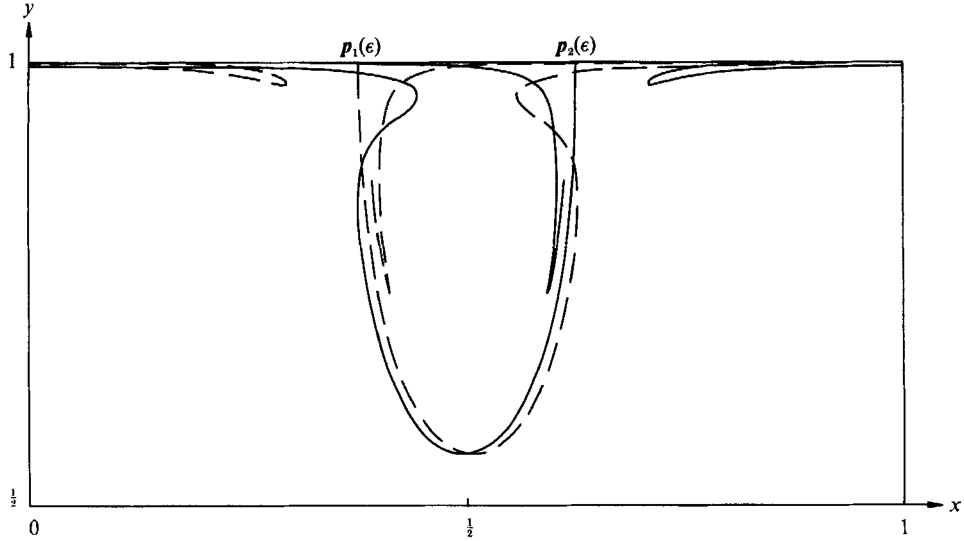

FIGURE 5. Stable $W^s_\epsilon(p_2)$ and unstable $W^u_\epsilon(p_1)$ manifolds of the fixed points of the Poincaré map $P^{t_0}_\epsilon$, denoted by continuous and broken curves respectively, for $U = 17/24$, $A = 1/\pi$ and $\epsilon = 0.01$.

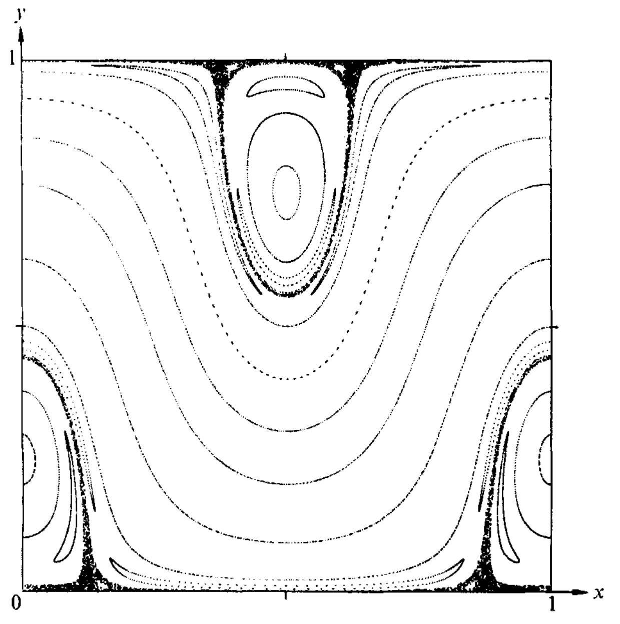

FIGURE 6. Two chaotic orbits and 14 non-chaotic orbits of P^0_ϵ for $U = 17/24$, $A = 1/\pi$ and $\epsilon = 0.001$; the starting points of the chaotic orbits were at $x = 0.375$, $y = 0.9999$, and $x = 0.122$, $y = 0.00001$, and 10000 iterates for each are shown.

regions. Figure 6 illustrates these phenomena, showing the iterations of a Poincaré map for several initial conditions when $\epsilon = 0.001$. Recall that if a particle is advected across $x = 0$ or $x = 1$ we use, for convenience, the periodic condition to plot it inside the square.

In addition to the chaotic regions associated with the breakup of the heteroclinic orbits, KAM theory shows that for all $\epsilon \neq 0$ there are stochastic layers due to the

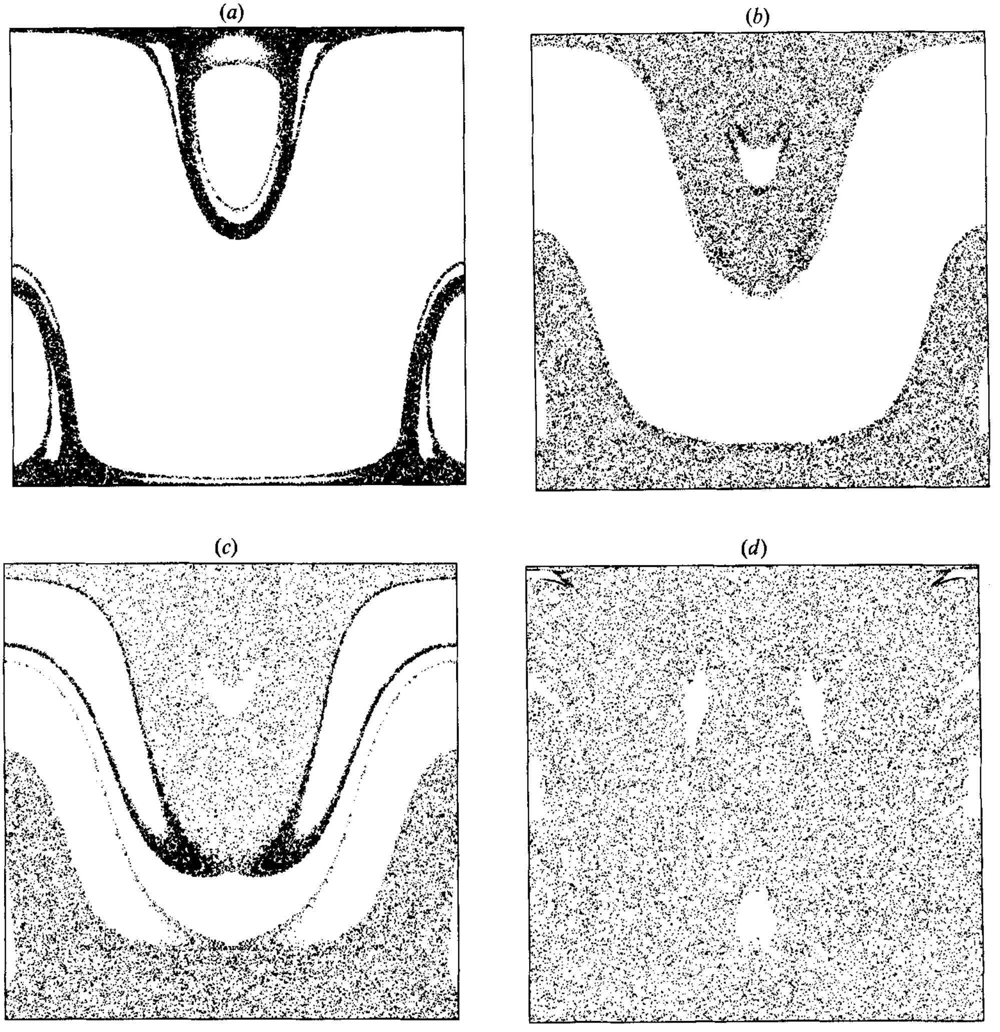

FIGURE 7. Chaotic orbits of P_ϵ^0 for $U = 17/24$ and $A = 1/\pi$; 10000 iterates of each of two orbits in the unit square of the (x, y)-plane are shown for each of the following cases: (*a*) $\epsilon = 0.005$, (*b*) $\epsilon = 0.05$, (*c*) $\epsilon = 0.06$, (*d*) $\epsilon = 0.4$.

breakup of resonant tori, i.e. tori with rational winding numbers. For example, consider a torus with winding number $1/n$, where n is some positive integer. The perturbation destroys all but an even number of the periodic orbits on the torus, thereby breaking the torus. Half of the preserved periodic orbits are of elliptic-type stability: the n points defining each orbit on the Poincaré map are each surrounded by islands of closed curves. The remaining preserved periodic orbits are of saddle-type instability, and have associated stable and unstable manifolds. These manifolds are confined between neighbouring irrational tori, which are preserved for sufficiently small ϵ. Generically, these manifolds intersect transversely an infinite number of times; as do the perturbed manifolds associated with a heteroclinic orbit, so forming a chaotic layer. As ϵ is increased, the tori with irrational winding numbers are also destroyed and neighbouring chaotic layers merge. Then the volume of phase space accessible to a single chaotic solution will suddenly increase.

Figure 7 (*a*) for $\epsilon = 0.005$ illustrates this: a chaotic solution, whose initial point is in the heteroclinic tangle, wanders over two surrounding layers which have merged. Consider the upper chaotic region. The unperturbed system contained two resonant tori near Γ_0 with winding number $\frac{1}{2}$, one just inside Γ_0 winding around $\boldsymbol{c}_1$, the other in the main stream just outside Γ_0. The perturbation breaks these tori and forms stochastic layers, leaving just two period-two orbits associated with each torus. The islands surrounding the two points defining the elliptic-type orbits on the Poincaré map are clearly visible in the figure. Those associated with the breakup of the enclosed resonant torus lie across the line $x = \frac{1}{2}$, while those associated with the outer resonant torus lie near the main stream symmetrically on each side of $x = \frac{1}{2}$. The symmetry of the system under the transformation T_1 implies that corresponding structures occur in the chaotic region associated with the lower heteroclinic orbit. Similarly, figure 7 (*c*) shows the islands and saddle points associated with the breakup of zonal tori with unit winding number.

As ϵ is increased further, the chaotic region accessible to a single orbit grows as successive stochastic layers merge. Finally, the last zonal barrier is broken, at $\epsilon \approx 0.24$ for the parameter values used in our numerical experiments, and the upper and lower chaotic regions merge. However, as is shown in figure 7 (*d*), a single solution may still not have access to the entire phase space because some islands of tori remain.

Another important feature of the flow, which is evident from our numerical results, is the presence of 'cantori'. These are Cantor sets which are invariant under $\mathrm{P}_\epsilon^{t_0}$; they form partial barriers in the chaotic regions of phase space. The theory of Hamiltonian systems shows that cantori appear, replacing invariant tori which form complete barriers, when a twist map is perturbed (Katok 1983). Our unperturbed map $\mathrm{P}_0^{t_0}$ can be thought of as three twist maps patched together along Γ_0 and along the image of Γ_0 under T_1; one in each region of recirculation, corresponding to twist maps on discs around the points $\boldsymbol{c}_1$ and $\boldsymbol{c}_2$; the third in the area of free flow, corresponding to a twist map around the circumference of a cylinder. So it is not surprising that cantori occur in our model flow. Moreover, since this application of twist maps does not depend on the details of the model, we anticipate that cantori will occur generally for Rossby waves and impede the spread of chaotic orbits.

For example, the heteroclinic tangle and the period-one stochastic band merge for some value of ϵ between 0.05 and 0.06. When $\epsilon = 0.05$ (figure 7 *b*) invariant tori form a zonal barrier between the two chaotic regions. When $\epsilon = 0.06$ (figure 7 *c*) the regions have merged, yet a partial barrier exists in the region previously occupied by the tori; the evidence for this is that an orbit starting in the region of the stochastic band takes a long time (about 1000 iterations) to penetrate the region of the heteroclinic tangle. The approximate position of the cantorus is shown, by the sudden change in density of points, in the upper orbit of figure 7 (*c*).

We return now to the properties of the transport of particles by the Rossby waves; qualitatively similar flows have been studied by Weiss & Knobloch (1989). The chaotic orbits appear to be stochastic, so it is interesting to investigate the existence of an effective diffusion coefficient D for particles moving within a given chaotic region. To do so, we no longer regard the flow as being confined to a cylinder, but allow x to take all real values, so that particles may be advected along an infinite channel. Using well-known ideas in the theory of longitudinal dispersion, we calculate

$$D_t = \{\langle(x_0 - x_t)^2\rangle - \langle(x_0 - x_t)\rangle^2\}/2t,$$

where x_0 is the initial coordinate of a particle and x_t is the coordinate of the particle

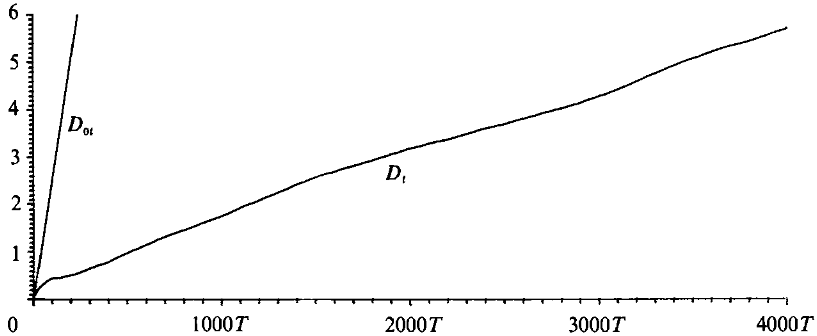

FIGURE 8. The graphs of D_t and D_{0t} versus t for particles in the upper chaotic region for two Rossby waves when $U = 17/24$, $A = 1/\pi$ and $\epsilon = 0.05$.

at time t. The averages, denoted by $\langle\ \rangle$, are taken over an ensemble of initial positions within a given chaotic region. We have computed D_t for the region of the heteroclinic tangle which lies near the unperturbed orbit Γ_0. The initial positions of 1000 particles were chosen at random in the chaotic region. The paths of the particles were then followed for 4000 time periods of the flow, and D_t was computed for $t = T, 2T, \ldots, 4000T$. Some typical results are shown in figure 8.

For a diffusion-limited process there exists $\lim_{t\to\infty} D_t = D$, say, the diffusion coefficient. This behaviour has been observed in a model of wavy Taylor vortices (Broomhead & Ryrie 1988), which is analogous to our problem with zero mean flow. However, our calculations for the Rossby waves with non-zero mean flow show that D_t increases apparently without limit as $t\to\infty$. This is akin to the behaviour of a simple shear flow, for which $D_t \sim t$ as $t\to\infty$. Indeed, Weiss & Knobloch (1989) attribute this anomalous behaviour to the presence of shear in the main stream. This is a plausible interpretation of our results also. Particles alternate intermittently between being carried along with the main stream and being trapped in the regions of recirculation. Thus we might expect D_t to be less than D_{0t} for all t, where D_{0t} is the value of D_t computed for the same initial conditions as D_t but with $\epsilon = 0$, i.e. the value when the particles are advected downstream by the first Rossby wave alone. This appears to be so in all the cases we have studied. We conclude that the perturbation causes mixing of fluid within a (restricted) chaotic region, and retards the downstream transport of the fluid in that region.

4. The combination of chaotic advection and molecular diffusion

We have hitherto regarded particles as passively moving with the fluid. However, in interpreting the results of chaotic advection, it must be recognized that solutes diffuse and solid particles move relative to the fluid locally. Khakhar & Ottino (1986) have considered the mixing of fluid by stretching in chaotic advection, and Aref & Jones (1989) have broached the issue of the separation of diffusing particles by chaotic advection. Here we examine further the combination of the effects of chaotic advection and molecular diffusion on the transport of a solute such as a dye in a real fluid, using order-of-magnitude estimates. Consider first the stretching and folding mechanism essential to chaotic advection, illustrated, for example, in figure 3. The mechanism corresponds to the existence of a horseshoe in some iterate, say the pth, of the Poincaré map (cf. Guckenheimer & Holmes 1986; Bertozzi 1988). Thus the flow stretches and folds a blob of dye into layers of discrete filaments. The distance between adjacent filaments decreases by a factor of, say, $\mu > 1$ after each iteration of the horseshoe map. Thus after a time npT the separation of filaments is

$$\delta \approx L\mu^{-n},$$

where L is the diameter of the region (and n is not so small that the size of the blob is important). Now molecular diffusion will smear adjacent filaments together provided that

$$\delta \lesssim (\kappa npT)^{\frac{1}{2}},$$

where κ is the coefficient of molecular diffusivity of the dye in the fluid. Therefore, the filaments will merge, and the dye will be uniformly diffused in the chaotic region after a time of order of magnitude t, where

$$\frac{2t}{pT}\ln\mu + \ln\left(\frac{t}{pT}\right) \gtrsim \ln\left(\frac{L^2}{\kappa pT}\right),$$

i.e.

$$\frac{2t}{pT}\ln\mu \gtrsim \ln\left(\frac{L^2}{\kappa pT}\right),$$

approximately, when the Péclet number $L^2/\kappa pT$, and therefore t/pT, is large. Note that L, p and T depend on the kinematics of the flow, and κ upon the dye and the fluid.

Thus chaotic advection, with its exponentially rapid dispersion by stretching and folding, enhances molecular diffusion so powerfully that dye will spread rapidly throughout a chaotic region unless the Péclet number is very large indeed. Moreover, the time for the dye to spread uniformly over the chaotic region is insensitive to the diffusivity of the dye (because of the logarithmic dependence on the Péclet number). This phenomenon was observed experimentally by Solomon & Gollub (1988), who found rapid diffusion whatever dye or liquid they used in oscillatory two-dimensional Rayleigh–Bénard convection.

5. Conclusions

The example of §2 proves the point that an unsteady potential flow may admit chaotic advection. It also illustrates very simply the kinematics of fluid transport across a separatrix of a steady flow owing to chaotic advection induced by an unsteady perturbation of the flow. These kinematics gain importance in the context of periodic flows such as wavy Taylor vortices, oscillatory Rayleigh–Bénard convection or waves in fluids. The example of §3 shows how this behaviour can lead to mixing of the fluid in a given chaotic region of the flow. A practical implication of this is that if a pollutant (e.g. radioactive particles) is released instantaneously at a point in a chaotic region then there is mild pollution by fallout over a large area, whereas if it is released at a point elsewhere (i.e. at an invariant point or an invariant curve of the Poincaré map) then there is intense pollution over a small area.

The Melnikov theory has been used to demonstrate the origin of dispersion in the examples of oscillating flows. It predicts the separation d_ϵ of the manifolds, and thereby the flux of fluid across a separatrix of the flow owing to the periodic perturbation. Thus it is useful not only in asserting the chaotic nature of the flow but also in finding approximations to the transport properties.

The important feature which leads to chaotic advection is the breaking of heteroclinic orbits. Their structural instability suggests that they are broken by most perturbations of the steady basic flow in which they arise. Then there are two possibilities: either the perturbed manifolds do not intersect, or they intersect at an infinite number of discrete points. The latter property leads to chaotic advection, as our calculations exemplify. However, we now see that this is a natural consequence of the incompressibility of the fluid. For consider a closed region of recirculation in the unperturbed flow of §3. There is no flux into this region; in particular there is no flux across the streamline Γ_0. In the perturbed flow there can be no net flux across any curve C joining the saddle points $\boldsymbol{p}_1(\epsilon)$ and $\boldsymbol{p}_2(\epsilon)$. Note also that there can be no net flux across any segment of the perturbed manifolds $W^{\mathrm{u}}_{\epsilon}(\boldsymbol{p}_1)$ and $W^{\mathrm{s}}_{\epsilon}(\boldsymbol{p}_2)$. Therefore if we take C as following $W^{\mathrm{u}}_{\epsilon}(\boldsymbol{p}_1)$ near $\boldsymbol{p}_1$ and $W^{\mathrm{s}}_{\epsilon}(\boldsymbol{p}_2)$ near $\boldsymbol{p}_2$, the two manifolds intersect at least once in the interior of the flow. Similarly, in the irrotational flow of §2 there can be no net flux of fluid in the y-direction provided the perturbation does not introduce additional sources or sinks. Thus there is no net flux across any curve joining the (horizontal) line of saddle points, so again the perturbed manifolds are constrained to intersect. This shows that chaotic advection occurs quite generally in flows with saddle-type stagnation points.

S.M.C. and K.S. thank SERC for their research studentships and S.C.R. thanks SERC for her research assistantship.

REFERENCES

AREF, H. 1984 Stirring by chaotic advection. *J. Fluid Mech.* **143**, 1–22.

AREF, H. & JONES, S. W. 1989 Enhanced separation of diffusing particles by chaotic advection. *Phys. Fluids* A **1**, 470–474.

ARNOL'D, V. 1965 Sur la topologie des écoulements stationnaires des fluides parfaits. *C. R. Acad. Sci. Paris* **261**, 17–20.

BATCHELOR, G. K. 1959 Small-scale variation of convected quantities like temperature in turbulent fluid. Part 1. General discussion and the case of small conductivity. *J. Fluid Mech.* **5**, 113–133.

BATCHELOR, G. K. 1967 *An Introduction to Fluid Mechanics*. Cambridge University Press.

BERTOZZI, A. 1988 Heteroclinic orbits and chaotic dynamics in planar fluid flows. *SIAM J. Math. Anal.* **19**, 1271–1294.

BROOMHEAD, D. S. & RYRIE, S. C. 1988 Particle paths in wavy vortices. *Nonlinearity* 1, 409–434.

CRAIK, A. D. D. & CRIMINALE, W. O. 1986 Evolution of wavelike disturbances in shear flows: a class of exact solutions of the Navier–Stokes equations. *Proc. R. Soc. Lond.* A **406**, 13–26.

DOMBRE, T., FRISCH, U., GREENE, J. M., HÉNON, M., MEHR, A. & SOWARD, A. M. 1986 Chaotic streamlines in the ABC flows. *J. Fluid Mech.* **167**, 353–391.

DRAZIN, P. G., BEAUMONT, D. N. & COAKER, S. A. 1982 On Rossby waves modified by basic shear, and barotropic instability. *J. Fluid Mech.* **124**, 439–456.

EADY, E. A. 1949 Long waves and cyclone waves. *Tellus* **1**, 33–52.

GRIFFEL, D. H. 1981 *Applied Functional Analysis*. Ellis Horwood.

GUCKENHEIMER, J. & HOLMES, P. 1986 *Nonlinear Oscillations, Dynamical Systems, and Bifurcations of Vector Fields*. Springer.

HÉNON, M. 1966 Sur la topologie des lignes de courant dans un cas particulier. *C. R. Acad. Sci. Paris* **262**, 312–314.

HOLTON, J. R. 1979 *An Introduction to Dynamic Meteorology*. Academic.

JONES, S. W. & AREF, H. 1988 Chaotic advection in pulsed source–sink systems. *Phys. Fluids* **29**, 469–485.

KATOK, A. 1983 Periodic and quasi-periodic orbits for twist maps. *Lecture Notes in Physics*, vol. 179, pp. 47–65. Springer.

KHAKHAR, D. V. & OTTINO, J. M. 1986 Fluid mixing (stretching) by time periodic sequences for weak flows. *Phys. Fluids* **29**, 3503–3505.

LORENZ, E. N. 1963 Deterministic nonperiodic flow. *J. Atmos. Sci.* **20**, 130–141.

ROM-KEDAR, V. 1989 Transport in two-dimensional maps. Ph.D. thesis, Cal. Inst. Tech.

RYRIE, S. C. 1990 Mixing by chaotic advection in spatially periodic flows. *J. Fluid Mech.* (submitted).

SOLOMON, T. H. & GOLLUB, J. P. 1988 Chaotic particle transport in time-dependent Rayleigh–Bénard convection. *Phys. Rev.* A **38**, 6280–6286.

TAYLOR, G. I. 1953 Dispersion of soluble matter in solvent flowing slowly through a tube. *Proc. R. Soc. Lond.* A **219**, 186–203.

WEISS, J. B. & KNOBLOCH, E. 1989 Mass transport and mixing by modulated travelling waves. *Phys. Rev.* A **40**, 2579–2589.